



JGR Solid Earth

RESEARCH ARTICLE

10.1029/2019JB018964

Key Points:

- Thick sediments reduce slab dip and increase seismogenic zone width and maximum earthquake magnitude
- Thick sediments also favor splay over outer rise faulting and partial over complete megathrust ruptures
- Simulation of long-term subduction dynamics and sediments significantly increases the estimated maximum magnitude of the megathrust

Supporting Information:

- Supporting Information S1
- Movie S1

Correspondence to:

S. Brizzi,
silvia.brizzi@uniroma3.it

Citation:

Brizzi, S., van Zelst, I., Funiciello, F., Corbi, F., & van Dinther, Y. (2020). How sediment thickness influences subduction dynamics and seismicity. *Journal of Geophysical Research: Solid Earth*, 125, e2019JB018964. <https://doi.org/10.1029/2019JB018964>

Received 5 NOV 2019

Accepted 9 JUN 2020

Accepted article online 15 JUN 2020

How Sediment Thickness Influences Subduction Dynamics and Seismicity

Silvia Brizzi^{1,2,3} , Iris van Zelst^{4,5} , Francesca Funiciello¹, Fabio Corbi^{1,6,7} , and Ylona van Dinther^{4,8} 

¹Laboratory of Experimental Tectonics, University of Roma Tre, Rome, Italy, ²Natural and Experimental Tectonics Research Group, University of Parma, Parma, Italy, ³Now at Jackson School of Geosciences, University of Texas at Austin, Austin, TX, USA, ⁴Department of Earth Sciences, Seismology and Wave Physics, Institute of Geophysics, ETH Zürich, Zürich, Switzerland, ⁵Now at Institute of Geophysics and Tectonics, School of Earth and Environment, University of Leeds, Leeds, UK, ⁶Department of Earth Sciences, Institute of Geological Sciences, Freie Universität Berlin, Berlin, Germany, ⁷Helmholtz Centre Potsdam - GFZ German Research Centre for Geosciences, Potsdam, Germany, ⁸Department of Earth Sciences, Utrecht University, Utrecht, The Netherlands

Abstract It has long been recognized that sediments subducting along the megathrust influence the occurrence of giant ($M_w \geq 8.5$) megathrust earthquakes. However, the limited observation span and the concurrent influence of multiple parameters on megathrust behavior prevent us from understanding how sediments affect earthquake size and frequency. Here, we address these limitations by using two-dimensional, visco-elasto-plastic, seismo-thermo-mechanical numerical models to isolate how sediment thickness affects subduction geometry and seismicity. Our results show that increasing sediment thickness on the incoming plate results in a decrease of the slab dip, as the trench retreats due to the seaward growth of the sedimentary wedge that also unbends the slab. This decrease in megathrust dip results in a wider seismogenic zone, so that the maximum magnitude of megathrust earthquakes increases. Concurrently, the recurrence time of characteristic events increases and partial ruptures are introduced. The maximum magnitude estimated for subduction segments with the thickest sediment input (Makran, West-Aegean, and Calabria) is distinctly higher than the instrumentally recorded magnitude. These segments may thus experience larger than as of yet observed earthquakes, albeit infrequently. Increasing sediment thickness also decreases megathrust normal stresses, as the seismogenic zone is more shallow and overlain by a lighter forearc structure. Thicker incoming plate sediments also favor more splay fault activity, whereas we observe more outer rise events for low sediment thickness. Finally, we demonstrate that modeling long-term subduction dynamics and sediment subduction is crucial for understanding and quantifying megathrust seismicity and seismic potential of subduction zones.

1. Introduction

The world's largest earthquakes ($M_w \geq 8.5$; hereafter giant earthquakes) are generally associated with interplate slip along the subduction megathrust. As recently demonstrated by the 2004 M_w 9.0 Sumatra-Andaman, 2010 M_w 8.8 Maule, and 2011 M_w 9.0 Tōhoku-Oki earthquakes, these big events cause severe damage in densely populated areas. Despite the recent advances in instrumental observations and analysis techniques, the fundamental processes controlling the size and temporal occurrence of megathrust earthquakes are still poorly understood.

The sediment thickness at the trench (Figure 1), possibly representative of the amount of sediments within the subduction channel, appears to play an important role in the maximum magnitude of interplate earthquakes. Ruff (1989) first noticed that the magnitude of megathrust events tends to be larger in sediment-rich margins. This led to the idea that the subduction of thick piles of sediments smoothes the interface, which results in uniform coupling that allows ruptures to propagate for large distances along strike (Ruff, 1989). Statistical analyses of updated and larger data sets have strengthened this hypothesis, showing that the majority of giant earthquakes occur in subduction segments with a trench sediment thickness greater than 1 km (Brizzi et al., 2018; Heuret et al., 2012; Ruff, 1989). Recently, Seno (2017) compiled the thickness of subducted sediments beneath the forearc wedge for different subduction segments and observed that regions where this thickness is lower than 1.2 km have never hosted giant events. A growing body of research

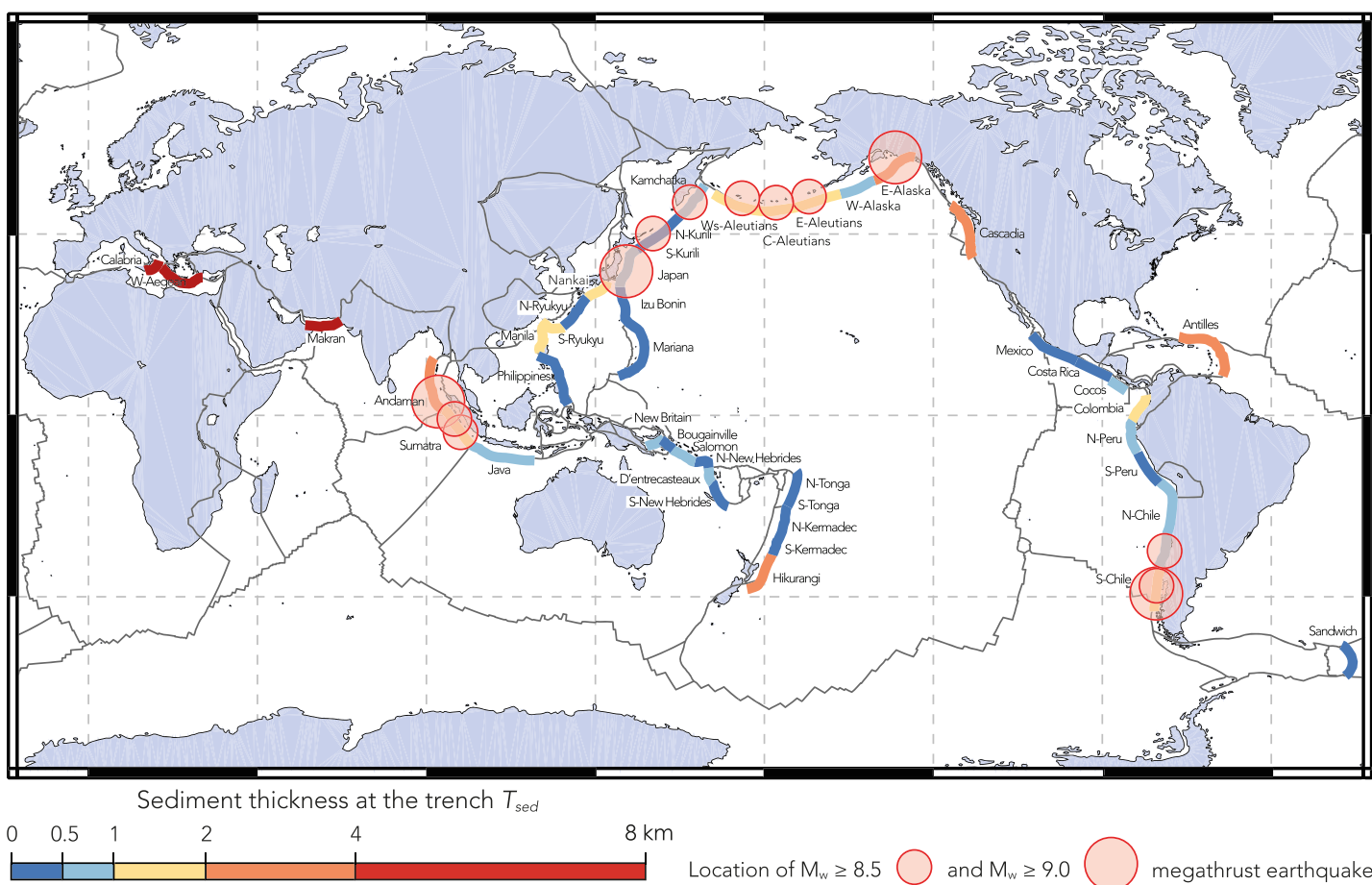


Figure 1. Global map showing the spatial relationship between trench sediment thickness T_{sed} and giant ($M_w \geq 8.5$) megathrust earthquakes. The color bar shows trench sediment thickness as defined by Heuret et al. (2012). Giant events since 1900 are from the ISC-GEM catalogue (see Brizzi et al., 2018, and references therein).

indicates that physical and geometrical properties of the plate interface are first-order controls on the seismogenic behavior of the subduction megathrust (Wang & Bilek, 2014). Indeed, it has been recently shown that subduction zones that have produced giant earthquakes tend to have a rather smooth incoming seafloor (Lallemand et al., 2018; van Rijsingen et al., 2018), likely because of a thick layer of sediments covering the interplate morphology.

Subducted sediments also influence the frictional properties of the megathrust. Laboratory experiments have demonstrated that both clay-rich material and ocean-floor carbonates are (frictionally) weak under a variety of conditions (e.g., Saffer & Marone, 2003). Moreover, the presence of fluids, particularly at high pressures, can weaken the megathrust by reducing the effective normal stress. Sediments are therefore thought to lubricate the plate interface (e.g., Lamb & Davis, 2003), thereby facilitating rupture propagation and large slip at shallow depths, as unexpectedly observed during the 2011 Tohoku-Oki earthquake (e.g., Sawai et al., 2014).

Regional observations suggest that the location of large megathrust events correlates with thick sediments at the interface (e.g., Gulick et al., 2011; Han et al., 2017; Olsen et al., 2020). However, the underlying physical mechanism responsible for this feedback is not yet fully understood. Having a century's worth of instrumental seismic record means that we only have a partial picture of the seismic cycle. Direct observations are restricted to the shallowest portion of the megathrust (e.g., Chester et al., 2012) or to exhumed subduction complexes (e.g., Fagereng, 2011), but linking these geological observations to seismicity is challenging. Furthermore, complexities introduced by different parameters acting simultaneously may hinder our

understanding of the role of sediment thickness and make it difficult to isolate its contribution on megathrust seismicity.

To overcome these observational limitations, we use two-dimensional, visco-elasto-plastic, seismo-thermo-mechanical (STM) models (van Dinther, Gerya, Dalguer, Corbi, et al., 2013; van Dinther, Gerya, Dalguer, Mai, et al., 2013; van Dinther et al., 2014) that are able to quantify the effects of incoming sediments on long-term subduction geometry and mechanics and short-term faulting. To investigate how sediment thickness affects subduction seismicity, we perform a parameter study where the incoming plate sediment thickness is systematically varied in agreement with recent estimates of natural subduction zones (Heuret et al., 2012). We characterize the role of sediments on the long-term evolution of convergent margins by analyzing kinematic, geometric, and mechanical features of our models. Then, we focus on the relationship between sediment thickness and megathrust seismicity by analyzing the maximum magnitude and recurrence times of interplate events. We also analyze how sediment thickness influences seismicity in the outer rise and sedimentary wedge regions. Finally, we quantify the effect of simulating sediments as a frictionally weak material by adapting the frictional properties of the megathrust. Despite unavoidable computational limitations, this study isolates and quantifies for the first time how incoming sediments affect both long-term subduction dynamics and subduction zone seismicity.

2. Seismo-Thermo-Mechanical Modeling

The STM modeling approach combines long-term subduction dynamics and short-term earthquake-like slip transients in a single framework (van Dinther, Gerya, Dalguer, Corbi, et al., 2013; van Dinther, Gerya, Dalguer, Mai, et al., 2013; van Dinther et al., 2014). First, the long-term evolution of a convergent margin resulting from the subduction of an oceanic slab beneath a continental plate is simulated using a time step of 1,000 years. At this stage, inertia is negligible, and friction remains constant. Once steady-state conditions are reached after ~9.7 Myr, the geometry, temperature field, and kinematics of the system remain almost unvaried (i.e., changes are negligible). In the short-term phase, the inertial term and a strongly slip rate-dependent friction formulation are activated to allow for frictional instabilities, as the time step is progressively decreased to 5 years (van Dinther, Gerya, Dalguer, Mai, et al., 2013). When the local pressure-dependent strength is reached over a large enough area, slip events occur spontaneously both on the megathrust and in the outer rise and sedimentary wedge regions (van Dinther et al., 2014). As slip velocity decreases, fault healing occurs, such that the fault strength is fully recovered.

2.1. Numerical Method

The STM modeling approach (van Dinther, Gerya, Dalguer, Corbi, et al., 2013; van Dinther, Gerya, Dalguer, Mai, et al., 2013) is based on the 2D continuum, thermomechanical code I2ELVIS (Gerya & Yuen, 2007), which uses an implicit, conservative finite difference scheme on a fully staggered Eulerian grid in combination with a Lagrangian marker-in-cell-technique. Conservation of mass, momentum, and energy are solved on the Eulerian grid using a visco-elasto-plastic rheology. Lagrangian markers advect physical properties (e.g., viscosity, stress, plastic strain, and temperature) according to the velocity field interpolated from the Eulerian grid (Gerya & Yuen, 2007). The momentum equations include the inertial term, which stabilizes high coseismic slip rates at small time steps (van Dinther, Gerya, Dalguer, Corbi, et al., 2013). Brittle failure is simulated with a Drucker-Prager plastic yielding criterion. At each Lagrangian marker, yielding occurs when the second invariant of the deviatoric stress tensor σ'_{II} reaches the local pressure-dependent yield strength σ_{yield} :

$$\sigma_{yield} = C + \mu(1 - \lambda)P, \quad (1)$$

where C is cohesion, μ is the effective slip rate-dependent friction coefficient, λ is the pore-fluid pressure factor (P_{fluid}/P), and P is pressure. Pore fluid pressure ratio's are 0.95 when fluid markers dehydrating from the slab and flowing according to pressure gradients are present (van Dinther, Gerya, Dalguer, Mai, et al., 2013).

Following van Dinther, Gerya, Dalguer, Corbi, et al. (2013), we use a strongly slip rate-dependent friction formulation (e.g., Ampuero & Ben-Zion, 2008) to introduce brittle instabilities and subsequent healing. At every Lagrangian marker, μ is calculated as a function of the visco-plastic slip rate V_{vp} as follows:

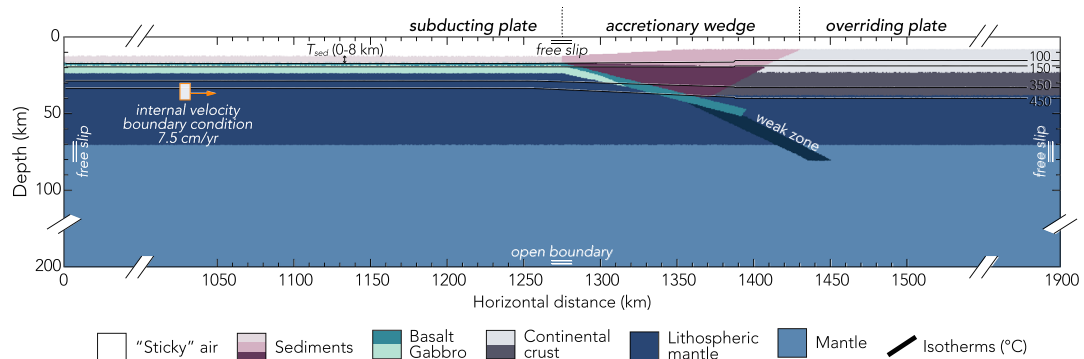


Figure 2. Model setup. Initial configuration of numerical models, including rock composition, temperature field (black lines), and boundary conditions (see section 2.3).

$$\mu = \mu_s(1 - \gamma) + \mu_s \left(\frac{\gamma}{1 + \frac{V_{vp}}{V_c}} \right). \quad (2)$$

Here, γ is the amount of slip rate-induced weakening, equivalent to $1 - \frac{\mu_s}{\mu_d}$. μ_s and μ_d are the static and dynamic friction coefficients corrected for the fluid pressure, respectively. V_c is the characteristic slip rate at which half of the friction drop occurs. Slip rate V_{vp} is calculated as the visco-plastic strain rate times a typical fault width:

$$V_{vp} = \left(\frac{\sigma_{yield}}{\eta_m} \right) \Delta x, \quad (3)$$

where η_m is the local viscosity and Δx the grid size. This formulation allows for spontaneous localization of the deformation at any orientation, both on- and off-megathrust (van Dinther et al., 2014). This means that rupture paths along the megathrust, as well as in the outer rise and sedimentary wedge, are governed by the local stress and strength conditions and not defined a priori. Full details of the method (van Dinther, Gerya, Dalguer, Corbi, et al., 2013; van Dinther, Gerya, Dalguer, Mai, et al., 2013) can be found in Text S1 in the supporting information.

2.2. Model Setup

The model setup is slightly modified from van Dinther, Gerya, Dalguer, Mai, et al. (2013) and resembles the Southern Chilean margin. In a $1,900 \times 200 \text{ km}^2$ trench-normal section, an oceanic plate subducts into the upper mantle beneath a continental plate and sedimentary wedge (Figure 2). To investigate the effect of subducting sediments, the oceanic crust is overlain by a sedimentary layer with thickness T_{sed} , which we vary from 0 km (i.e., no sediments) to 8 km. This range is in agreement with recent estimates provided in the database of Heuret et al. (2012).

The grid consists of $1,831 \times 270$ nodes. The spatial resolution is nonuniform, as the grid spacing varies from 500 m in our region of interest (i.e., the surroundings of the megathrust) to a maximum of 2,000 m elsewhere in the model. Seventeen million randomly distributed Lagrangian markers are used to advect materials and their physical properties.

The visco-elasto-plastic material parameters are based on laboratory rock experiments (Table 1) as described in van Dinther, Gerya, Dalguer, Mai, et al. (2013). For all lithologies, velocity weakening behavior occurs in the $150\text{--}350^\circ\text{C}$ temperature range (van Dinther, Gerya, Dalguer, Mai, et al., 2013). A linear transition to velocity strengthening behavior is imposed from 150°C to 100°C (thermal limits taken from, e.g., Hyndman et al., 1997). The brittle-ductile transition occurs self-consistently, as the temperature and stress distribution between $\sim 350^\circ\text{C}$ and $\sim 450^\circ\text{C}$ activate dislocation creep that decreases viscosity (van Dinther, Gerya, Dalguer, Mai, et al., 2013). Cohesion of the subduction megathrust, as well as of all other rock types, is

Table 1
Material Parameters

Material	Flow law ^a	η_0 [Pa ⁿ s]	n [–]	E_a [J mol ⁻¹]	V_a [J Pa ⁻¹]	ρ_0^b [kg m ⁻³]	G [GPa]	μ_s [–]	C [MPa]
Sticky air	—	$1.0 \cdot 10^{17}$	1	0	0	1	700	0	0
Sediments	Wet quartzite	$1.97 \cdot 10^{17}$	2.3	$1.54 \cdot 10^5$	$0.8 \cdot 10^{-5}$	2600	5	0.35 ^c	6
Upper oceanic crust	Wet quartzite	$1.97 \cdot 10^{17}$	2.3	$1.54 \cdot 10^5$	$0.8 \cdot 10^{-5}$	3000	12	0.50 ^d	6 ^h
Lower oceanic crust	Plagioclase	$4.80 \cdot 10^{22}$	3.2	$2.38 \cdot 10^5$	$0.8 \cdot 10^{-5}$	3000	12	0.85 ^e	6
Upper continental crust	Wet quartzite	$1.97 \cdot 10^{17}$	2.3	$1.54 \cdot 10^5$	$1.2 \cdot 10^{-5}$	2700	12	0.72 ^f	6
Lower continental crust	Wet quartzite	$1.97 \cdot 10^{17}$	2.3	$1.54 \cdot 10^5$	$1.2 \cdot 10^{-5}$	2700	12	0.72 ^f	6
Lithospheric mantle	Dry olivine	$3.98 \cdot 10^{16}$	3.5	$5.32 \cdot 10^5$	$0.8 \cdot 10^{-5}$	3300	35	0.60 ^g	6
Asthenospheric mantle	Dry olivine	$3.98 \cdot 10^{16}$	3.5	$5.32 \cdot 10^5$	$0.8 \cdot 10^{-5}$	3300	35	0.60 ^g	6
Mantle weak zone	Wet olivine	$5.01 \cdot 10^{20}$	4.0	$4.70 \cdot 10^5$	$0.8 \cdot 10^{-5}$	3300	63	0.10	6

Note. η_0 is the reference viscosity; n is the stress exponent; E_a is the activation energy; V_a is the activation volume; ρ_0 is the reference density; G is the shear modulus; μ_s is the static friction coefficient, and C is cohesion. See van Dinther, Gerya, Dalguer, Corbi, et al. (2013) for parameters related to the energy equation (Text S1).

^aRanalli (1995). ^bTurcotte and Schubert (2002). ^cDen Hartog et al. (2012). ^dDi Toro et al. (2011). ^eTsutsumi and Shimamoto (1997). ^fF. Chester and Higgs (1992). ^gDel Gaudio et al. (2009). ^hSchultz (1995).

assumed to be relatively low (6 MPa; Schultz, 1995) to reflect the significant fracturing that occurs during subduction. The pore fluid pressure factor λ of the sedimentary units is set to 0.95 in agreement with recent strength estimates (e.g., Seno, 2009), while hydrostatic conditions ($\lambda = 0.4$) are assumed for all other rock types. Fluid is also treated in a simplified manner compared to van Dinther, Gerya, Dalguer, Mai, et al. (2013), as their location only depends on the rock type.

2.3. Initial and Boundary Conditions

Subduction is kinematically driven by imposing a constant velocity of 7.5 cm/year within a small region of the subducting plate (Figure 2). Subduction is initiated by prescribing an initial weak zone (e.g., Gerya & Meilick, 2011) with low plastic strength and a wet olivine rheology. Free slip boundary conditions are applied at the top and side boundaries of the model, and we impose an open boundary condition at the bottom boundary (Gorczyk et al., 2007). The upper portion of the model is treated as an internal free surface by imposing a 12.5 km layer of “sticky air” (Crameri et al., 2012). This behaves as a purely viscous material, with a low viscosity (10^{17} Pa·s) and density (1 kg/m^3), and high shear modulus (700 GPa) (van Dinther, Gerya, Dalguer, Mai, et al., 2013).

The initial thermal structure of the oceanic lithosphere is calculated from the half-space cooling model (Turcotte & Schubert, 2002) for a 40 Myr old slab, while the initial temperature of the continental lithosphere linearly increases from $T = 0^\circ\text{C}$ at the surface to $T = 1,300^\circ\text{C}$ at 100 km depth. The thermal gradient of the mantle is adiabatic and set to 0.5°C/km .

2.4. Quantifying Long- and Short-Term Behavior

To quantify the effect of increasing incoming plate sediment thickness T_{sed} on long-term subduction behavior, we measure the dip of the megathrust at seismogenic zone depths θ_{sz} and the width of the seismogenic zone W_{sz} . To derive these parameters, we first define the depth of the updip and downdip limits of the seismogenic zone as the depth where the 150°C and 350°C isotherms (e.g., Hyndman et al., 1997) cross-cut the top of the basalt layer (Figure S1). We then measure θ_{sz} and W_{sz} using the angle with respect to the horizontal and the straight line connecting the updip and downdip limits of the seismogenic zone (Figure S1) (Heuret et al., 2011). This ensures comparison of our results with the global database of subduction zone parameters and interpolate seismicity (Heuret et al., 2011).

To analyze the short-term seismicity, we first identify and separate events with the Rupture Detector Algorithm (RDA) developed by Dal Zilio et al. (2018). At each timestep, the RDA identifies all the markers that move seaward at velocities larger than $6.5 \cdot 10^{-9}$ m/s and experience a stress drop larger than 0.4 MPa, which is a minimum stress drop estimate for moderate to large earthquakes (Allmann & Shearer, 2009). In our models, earthquakes are thus defined as events of localized plastic slip, which release elastically

accumulated stresses and permanently displace the overriding plate seaward. Based on the obtained data set, a connectivity matrix is then computed to evaluate the distance between rupturing markers during the analyzed time step or the previous one. If this distance is lower than 1.5 km, markers are grouped into one event. Subsequently, we calculate the rupture width W from a straight line between the events exterior points. The RDA thresholds have been selected such that events can be clearly detected. Using different values introduces slight variations to values of rupture width W , moment magnitude M_w and the number of events, but does not change any of our findings.

For each two-dimensional rupture, M_w is estimated using the empirical rupture width-magnitude scaling relationship defined for subduction zone earthquakes by Blaser et al. (2010):

$$M_w = 4.04 + 2.17\log(W), \quad (4)$$

where W is the rupture width measured in kilometers. The maximum moment magnitude M_{max} is subsequently defined as the maximum M_w observed during the short-term modeling stage (i.e., 25,000 years). The recurrence time τ is defined as the average time between all megathrust events, while we define τ_c as the average time span between characteristic events that rupture the complete seismogenic zone width.

3. Results

In the following, we outline the relationship between T_{sed} and long-term subduction dynamics (section 3.1) and short-term subduction seismicity (section 3.2). We then describe the results of an additional model where we tune the frictional properties of the megathrust as a proxy for the presence of sediments in the subduction channel (section 3.3).

3.1. Role of Sediment Thickness on Long-Term Subduction

The long-term behavior of our models is strongly dependent on T_{sed} , as we observe different modes of subduction (Figure 3). After subduction initiation along the weak zone, the model with $T_{sed} = 0$ km shows an initial phase (~ 2 Myr) where sediments are scraped off from the base of the sedimentary wedge. If $T_{sed} > 0$ km, this initial phase is instead characterized by sediment accretion at the frontal margin. As subduction continues, sediments are carried to an average depth of 100 km in a continuous subduction channel. At steady-state conditions after ~ 9.7 Myr, models with $T_{sed} < 1.5$ km display trench advance, such that the trench appears to be shifted towards the upper plate with respect to its initial location (Figures 3a and 3b). As T_{sed} increases, the trench migrates towards the subducting plate at increasing rates (Figure S2a). This retreating trench motion is not accompanied by slab retreat (i.e., seaward migration of the entire slab; Movie S1). The subduction interface at depth approximately remains at the same location, with a seaward shift of only ~ 25 km at a depth of 90 km when increasing T_{sed} from 1.5 to 8 km (Figures 3c and 3d).

The temperature field, geometry, and mechanical properties of the megathrust are also significantly affected by T_{sed} (Figure 4). For $T_{sed} = 0$ km, the updip and downdip limits of the seismogenic zone (approximated by the 150°C and 350°C isotherms) are located at ~ 20 and ~ 60 km depth (Figure 4a). For $T_{sed} = 8$ km, the seismogenic zone lies between ~ 10 and ~ 46 km depth (Figure 4a). Therefore, the depth of the megathrust seismogenic zone decreases distinctly with increasing T_{sed} (Figure 3). This approximate upward translation occurs for both the updip and downdip limits of the seismogenic zone, thus leaving the seismogenic depth range almost unvaried for $T_{sed} > 1$ km (Figure 4a).

Looking at the megathrust geometry, we observe that the slab dip at seismogenic zone depths θ_{sz} linearly decreases as a function of T_{sed} , with values ranging from 26° to $\sim 8^\circ$ ($R = -0.97$; Figure 4b). Our results also show that the downdip width of the seismogenic zone W_{sz} increases linearly from 81 to 255 km as T_{sed} increases ($R = 0.97$; Figure 4c).

To better understand the possible physical mechanisms responsible for the feedback between the amount of sediments and the long-term subduction behavior, we also analyze the yield strength of the sediment-basalt interface σ_{yield} at steady-state conditions. We measure σ_{yield} between the 150°C and 350°C isotherms at the bottom of the sedimentary layer, because this is where megathrust earthquakes preferentially propagate in our models. Results for increasing T_{sed} show that σ_{yield} is smaller across the entire depth range of the

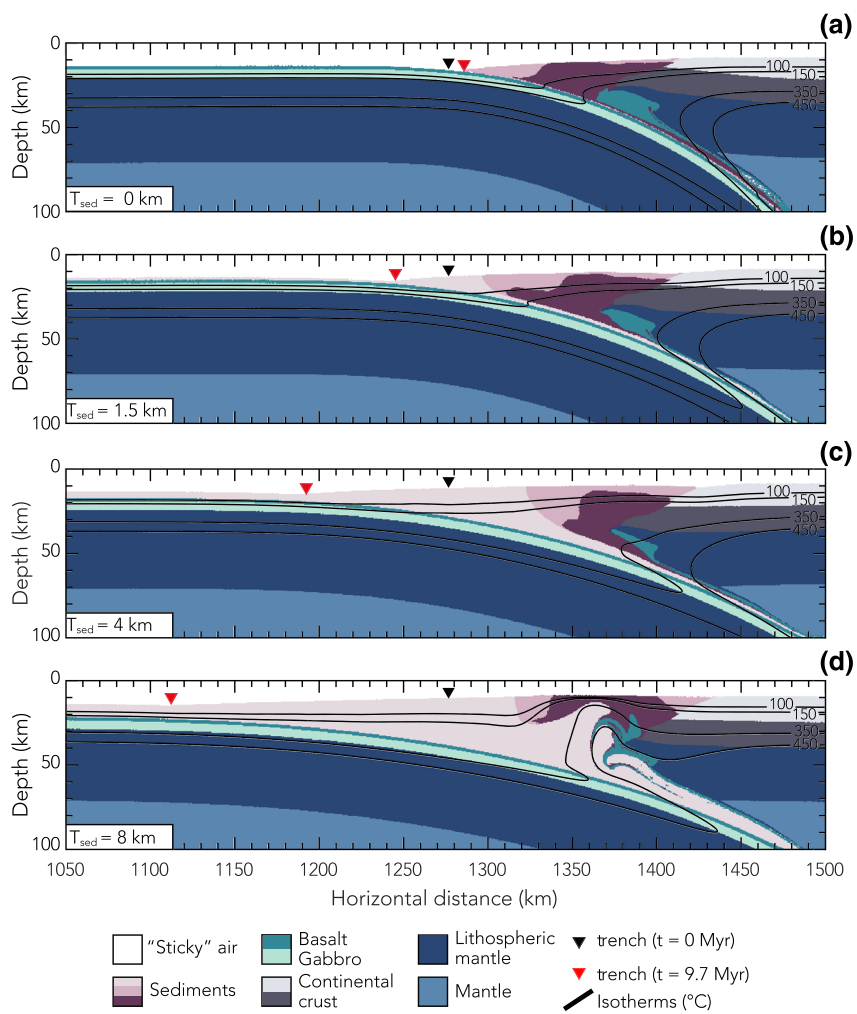


Figure 3. Configuration of the models with different sediment thickness T_{sed} after ~ 9.7 Myr of subduction. (a) $T_{\text{sed}} = 0 \text{ km}$, (b) $T_{\text{sed}} = 1.5 \text{ km}$, (c) $T_{\text{sed}} = 4 \text{ km}$, and (d) $T_{\text{sed}} = 8 \text{ km}$. The color scale refers to the rock composition. The black lines are isotherms. The black and red triangles mark the location of the trench at $t = 0 \text{ Myr}$ and $t = 9.7 \text{ Myr}$, respectively.

seismogenic zone (Figure 4d). This shows that models with thick sediments on the incoming plate have relatively weaker megathrusts.

3.2. Role of Sediment Thickness on the Short-Term Seismic Behavior

During the short-term evolution of our models, events propagate on- and off-megathrust (Figure 5). Megathrust earthquakes nucleate close to the downdip limit of the seismogenic zone, where plate coupling decreases spontaneously due to the brittle-ductile transition. The events propagate upward and partially break into the updip velocity-strengthening region.

Off-megathrust events occur both in the outer rise and the sedimentary wedge (Figure 5). Outer rise normal faults related to the bending of the slab occur between 50 km seaward and 30 km landward of the trench. They extend deep into the lithospheric mantle, but never to temperatures greater than 450°C . The majority of these faults dip trenchward at 60° – 70° , but seaward dipping antithetic planes develop as well. Blind splay faults occur between 100 and 200 km landward of the trench, branching off from the megathrust at a depth of ~ 30 km and propagating within the sedimentary wedge. Faults generally dip between 20° and 35° landward with an imbricate geometry, but steeply dipping ($\sim 70^{\circ}$) seismically active backthrusts are also present.

Off-megathrust seismicity is limited to the outer rise region for $T_{\text{sed}} = 0 \text{ km}$ (Figure 5a). In contrast, for $T_{\text{sed}} = 8 \text{ km}$, outer rise events are absent and off-megathrust earthquakes propagate exclusively within

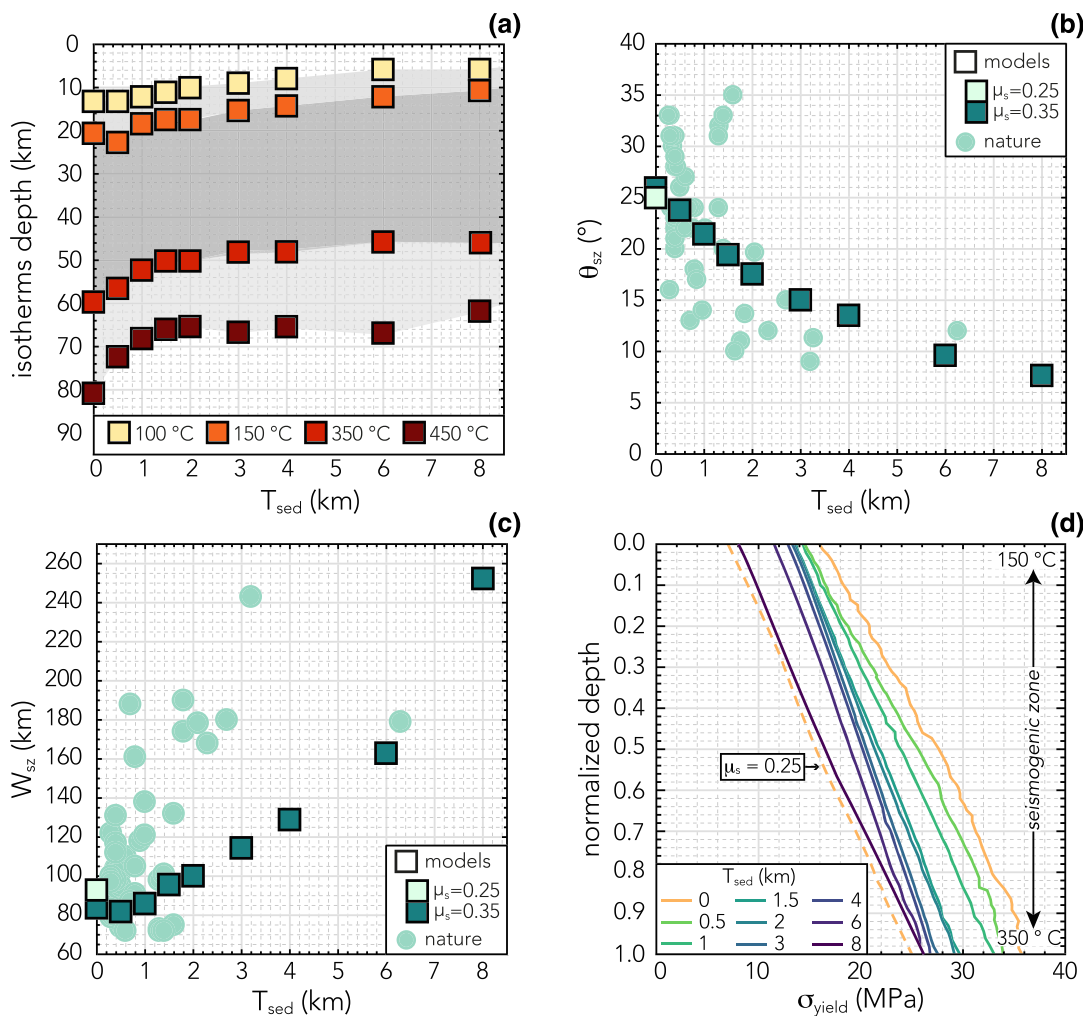


Figure 4. Long-term modeling results. (a) Temperature distribution, (b) dip of the megathrust θ_{sz} , (c) downdip width of the seismogenic zone W_{sz} , and (d) yield strength of the megathrust σ_{yield} at seismogenic zone depths as a function of the sediment thickness T_{sed} . The dark and light gray shaded areas in panel a highlight the location of the seismogenic zone and transition to the up-dip and downdip aseismic regions, respectively. The light green square in panels b and c refers to an additional model, where sediments are simulated by adapting the static friction coefficient μ_s of the megathrust (see section 3.3). For natural subduction zones, θ_{sz} and W_{sz} are from Heuret et al. (2011).

the sedimentary wedge (Figure 5d). The amount of sediments on the incoming plate thus influences the partition of seismic energy released off-megathrust. Indeed, the number of earthquakes in the slab bending area decreases as a function of T_{sed} , while there is a positive correlation between the number of splay faults within the sedimentary wedge and T_{sed} (Figure S3).

To explore how subducting sediments affect the interface seismicity, we first focus on the spatio-temporal evolution of megathrust earthquakes (Figure 6). As T_{sed} increases, we observe two different styles of seismicity. In the models with $T_{\text{sed}} \leq 4$ km, the megathrust ruptures in regular seismic cycles, with quasi-periodic and quasi-characteristic events that saturate the entire seismogenic zone width (Figures 6a–6c). The coefficient of variation CV of recurrence intervals, which is defined as the ratio of the standard deviation and the average recurrence time, is ≤ 0.3 . This confirms quasi-periodic behavior for $T_{\text{sed}} \leq 4$ km. In contrast, for $T_{\text{sed}} \geq 6$ km, smaller, partial ruptures occur in addition to large quasi-characteristic earthquakes (Figure 6d). In this case, CV is ≥ 0.8 , which indicates aperiodic behavior.

The maximum moment magnitude of megathrust events M_{max} increases linearly from 8.2 to 9.1 as a function of T_{sed} ($R = 0.95$; Figure 7a), which is consistent with the first-order control of T_{sed} on W_{sz} . The recurrence time of the characteristic events τ_c also increases linearly from 300 to 900 years for increasing

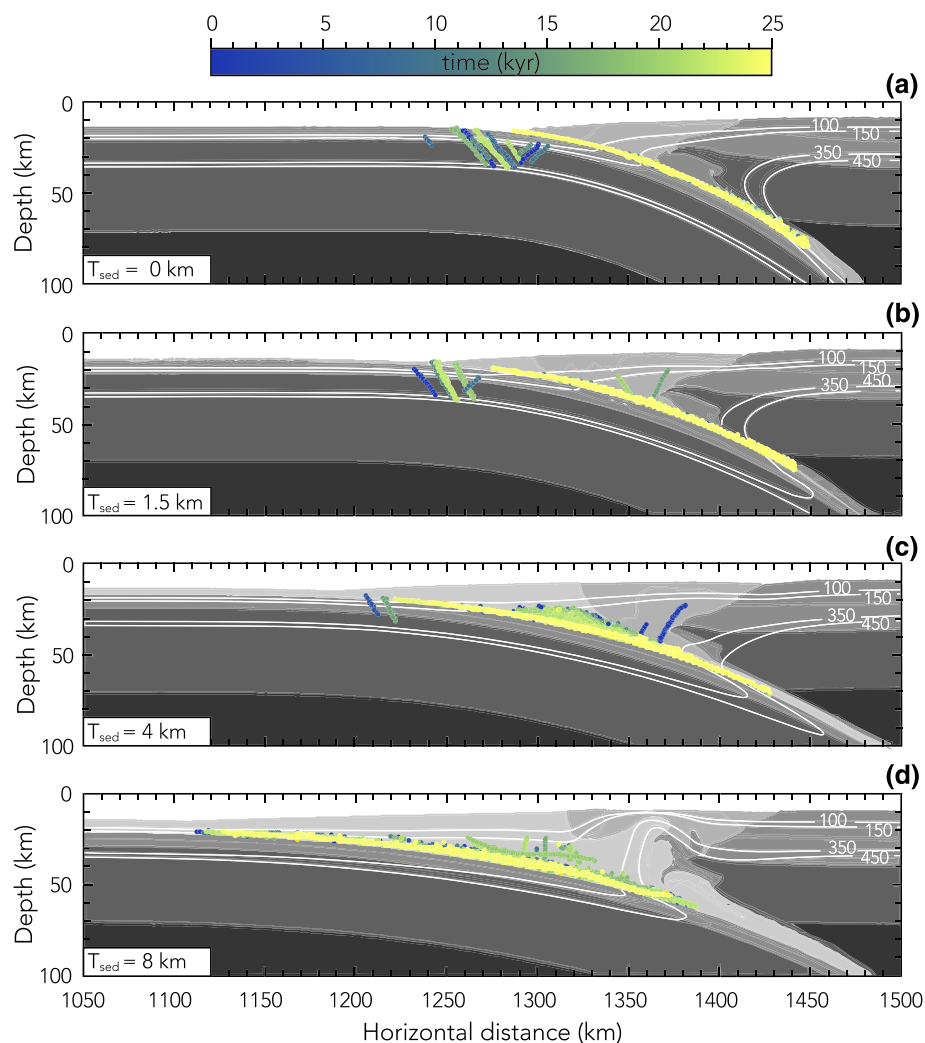


Figure 5. Spatial distribution of seismicity during 25,000 years of short-term model evolution for different sediment thickness T_{sed} . (a) $T_{\text{sed}} = 0 \text{ km}$, (b) $T_{\text{sed}} = 1.5 \text{ km}$, (c) $T_{\text{sed}} = 4 \text{ km}$, and (d) $T_{\text{sed}} = 8 \text{ km}$. Grayscale colors depict rock composition (see Figure 3).

T_{sed} ($R = 0.98$; Figure 7b). This is likely due to the increase of W_{sz} , which increases the time needed for stress build-up. When considering the overall seismicity of the megathrust, the recurrence time of the events τ deviates from the trend of characteristic earthquakes (i.e., $\tau \ll \tau_c$) for the models with $T_{\text{sed}} \geq 6 \text{ km}$ (Figure 7b), because of the occurrence of smaller events that partially rupture the seismogenic zone. The amount of sediments thus strongly influences megathrust seismicity. As the sediment thickness increases, the megathrust generates events of increasing maximum magnitude, but the time needed for these events to occur also increases. More importantly, megathrust behavior switches from a quasi-periodic to an irregular regime, with different-sized ruptures.

3.3. Role of Interface Friction on Megathrust Geometry and Maximum Earthquake Magnitude

Numerical studies often tend to simplify the presence of subducting sediments by only assuming a low static friction coefficient μ_s for the megathrust (e.g., Muldashev, 2017; Tan et al., 2012). We therefore test the scenario where incoming plate sediments are absent (i.e., $T_{\text{sed}} = 0 \text{ km}$) and instead parameterize the interface strength to mimic the weakening effect of sediments. More specifically, we run an end-member model with $T_{\text{sed}} = 0 \text{ km}$ and μ_s equal to 0.25 instead of 0.35. This value is chosen such that the effective

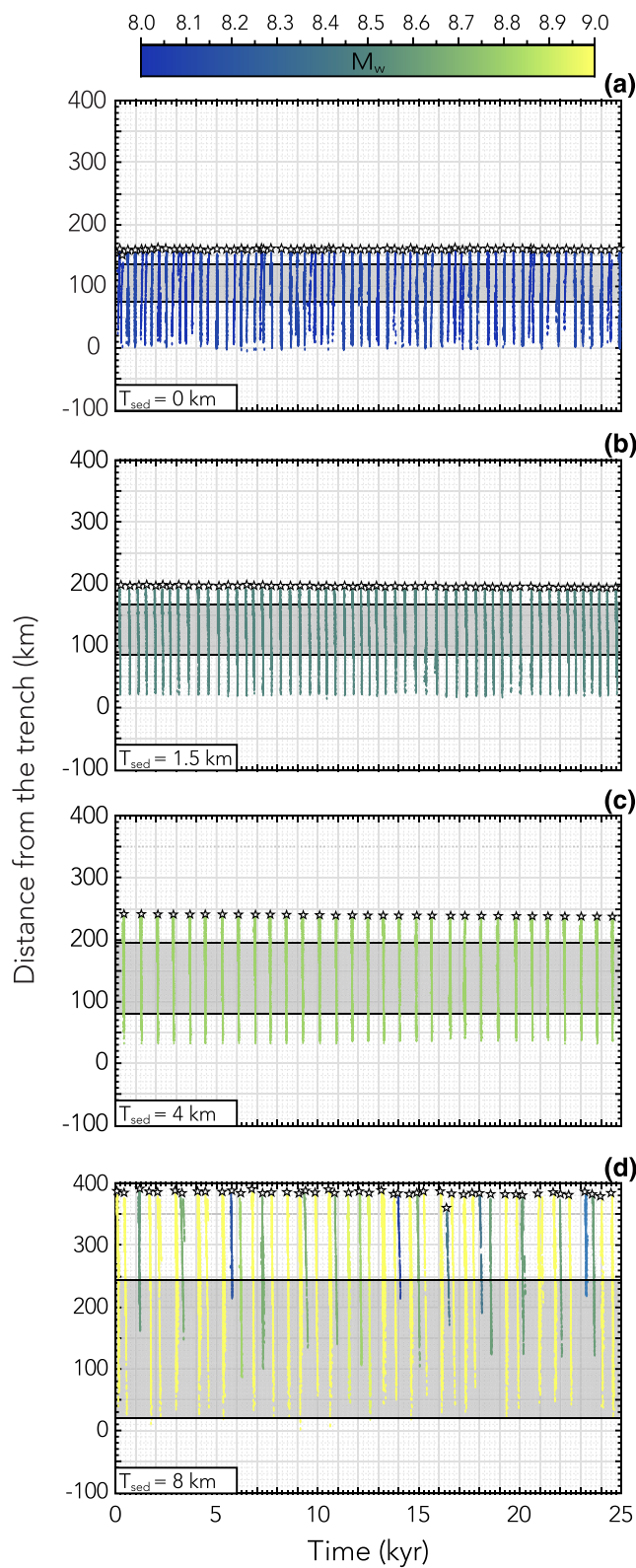


Figure 6. Spatio-temporal evolution of megathrust seismicity during 25,000 years of short-term model evolution for different sediment thickness T_{sed} . (a) $T_{\text{sed}} = 0 \text{ km}$, (b) $T_{\text{sed}} = 1.5 \text{ km}$, (c) $T_{\text{sed}} = 4 \text{ km}$, and (d) $T_{\text{sed}} = 8 \text{ km}$. The color scale refers to the moment magnitude M_w . The stars mark the location of the earthquake hypocenter. The gray rectangle marks the location of the seismogenic zone. The black lines mark the location of the up-dip and down-dip limits (i.e., 150°C and 350°C isotherms, respectively) of the seismogenic zone.

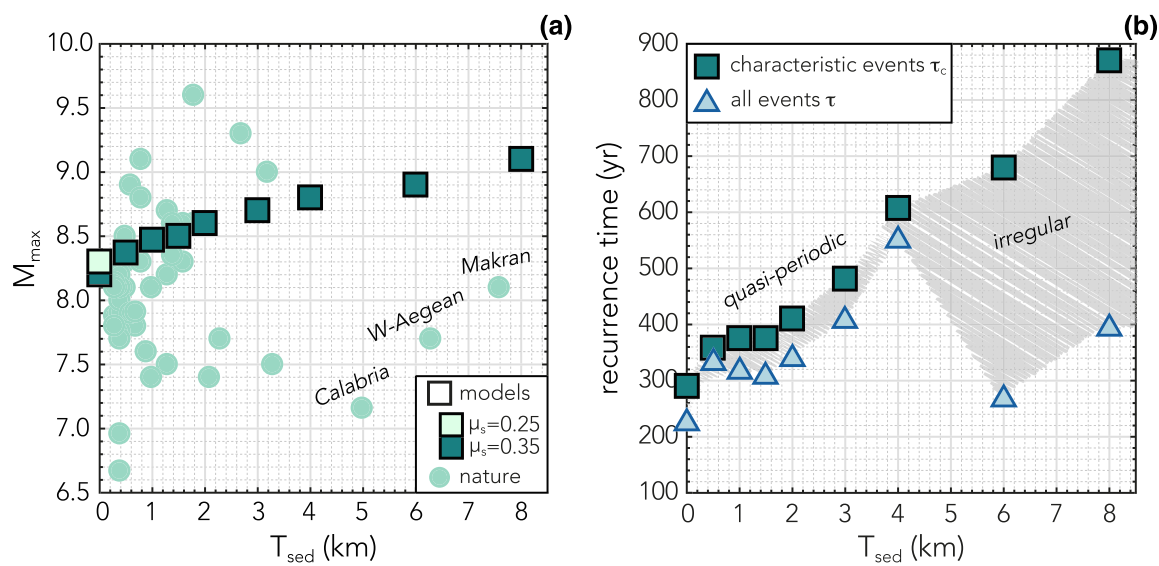


Figure 7. Megathrust behavior during 25,000 years of short-term model evolution. (a) Maximum moment magnitude M_{max} and (b) average recurrence time of characteristic τ_c and all events τ as a function of sediment thickness T_{sed} . The light green square in panel a refers to an additional model, where sediments are simulated by adapting the static friction coefficient μ_s of the megathrust (see section 3.3). For natural subduction zones, M_{max} is from the ISC-GEM catalog (see Brizzi et al., 2018, and references therein).

strength of the megathrust is similar to what is observed for the simulation with the thickest sediments (i.e., $T_{sed} = 8$ km; Figure 4d). This approach allows us to isolate the influence of including a physical layer of sediments.

The early phases of the long-term modeling stage are similar to the reference model with no incoming plate sediments. Subduction initiates along the weak zone, causing erosion at the base of the sedimentary wedge and subduction of these initial wedge sediments. At steady-state conditions after ~ 9.7 Myr, the trench has also advanced with respect to its initial location. The dip of the megathrust θ_{sz} is 25° (Figure 4b) and the downdip width of the seismogenic zone W_{sz} is 95 km (Figure 4c). By comparing the results of the models with $T_{sed} = 0$ km and different μ_s for the interface, we observe that varying T_{sed} results in a larger variability in terms of megathrust geometry than adapting μ_s . The decrease in slab dip is only $\sim 1^\circ$ for decreasing μ_s , while we observe a decrease of 17° when we increase T_{sed} (Figure 4b). This leads to an increase of the seismogenic zone width of only 14 km for decreasing μ_s instead of 174 km for increasing T_{sed} (Figure 4c).

Looking at the megathrust seismicity in this model where we only vary friction, we observe that M_{max} of megathrust earthquakes is 8.3. This means that the maximum magnitude has only increased by 0.1 (Figures 7a and 8). Increasing the amount of incoming plate sediments instead results in an increase of M_{max} of almost one order of magnitude (i.e., from ~ 8.2 to 9.1; Figures 7a and 8). Therefore, weakening the megathrust by only adapting the plate interface frictional properties to account for the presence of sediments results in a significant underestimation of the maximum size of interplate earthquakes.

4. Discussion

In this work, we show that long-term sediment subduction has strong effects on the evolution of convergent margins. These effects and the consequent impact on the short-term subduction seismicity are summarized in Figure 9.

In the following, we first discuss the limitations of our modeling approach (section 4.1). Then, we focus on the relationship between sediment thickness, long-term geometry, and the mechanical properties of the megathrust (section 4.2). We further discuss how incoming plate sediments affect megathrust (section 4.3) and off-megathrust seismicity (section 4.4). Finally, we show the importance of explicitly modeling

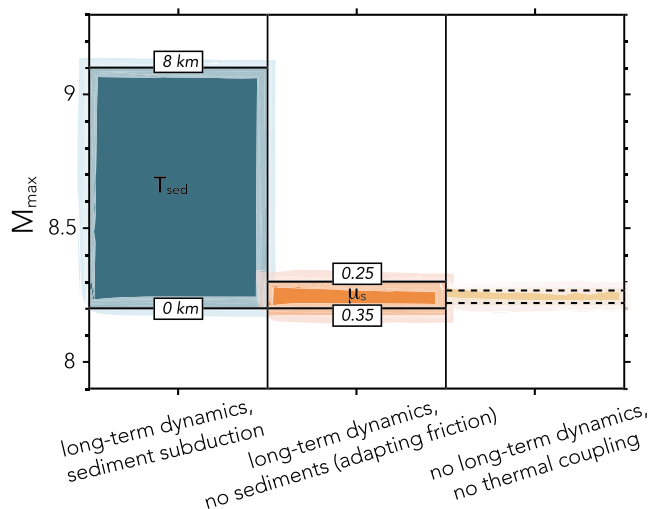


Figure 8. Effect of sediment thickness T_{sed} versus interface friction μ_s on the maximum magnitude M_{max} of megathrust earthquakes. M_{max} variation when incoming plate sediments are included as a physical layer (blue rectangle) or simulated only by tuning the frictional properties of the megathrust (orange rectangle). The last M_{max} range (light yellow rectangle) is hypothesized and derived assuming a simplified purely mechanical approach that does not include either long-term subduction dynamics or thermal coupling (see section 4.5).

sediments during long-term subduction (section 4.5) to obtain a better picture of megathrust behavior on shorter timescales, as well as the maximum earthquake magnitude.

4.1. Modeling Limitations

Our study substantiates previous suggestions that sediment thickness influences megathrust seismicity (e.g., Brizzi et al., 2018; Heuret et al., 2012; Ruff, 1989; Scholl et al., 2015; Seno, 2017). However, we caution that a single parameter could never explain the complex spatial distribution of giant earthquakes during the last century. Nonetheless, analyzing only one parameter allows us to isolate its specific contribution and better understand the physical processes and potential feedback mechanisms.

Earthquakes in nature occur in three-dimensional and structurally complex fault zones. Particularly, the trench-parallel extent of the subduction zone has an important control on the maximum magnitude of megathrust earthquakes. Indeed, the two biggest earthquakes of the last decades (i.e., 1960 Chile and 2004 Sumatra-Andaman earthquakes) have a large along-strike component, which is not taken into account in our 2D models. However, the empirical scaling relationship between downdip rupture width and M_w observed for subduction zone earthquakes does account for the feedback between trench-parallel and perpendicular rupture propagation (Blaser et al., 2010).

Due to the major numerical challenge of resolving both millions of years and subsecond time scales, events have an unrealistically long duration, as a large 5 year time step limits computations. This does not allow us to resolve earthquake nucleation and dynamics, which could affect the recurrence interval and slip distribution (van Zelst et al., 2019). However, the main findings of this paper are determined by long-term characteristics that are not affected by the limited time resolution of our approach.

We treat fluid flow processes in a simplified fashion, as pore fluid pressure only depends on rock type (see section 2.2). Pore fluid pressure is thought to affect fault strength and the mode of slip (e.g., Audet & Schwartz, 2013; Gao & Wang, 2017; Moreno et al., 2014, 2018). Fluids may also promote several geochemical processes that may result in the metasomatic alteration of subducting sediments, and thereby in changes of their physical, rheological, and frictional properties (e.g., Saffer & Tobin, 2011). Such complexities are not taken into account but are the subject of ongoing research (e.g., Gerya, 2019). By implementing the fluid flow component, we expect to gain additional information on the role of subducting sediments on megathrust seismicity.

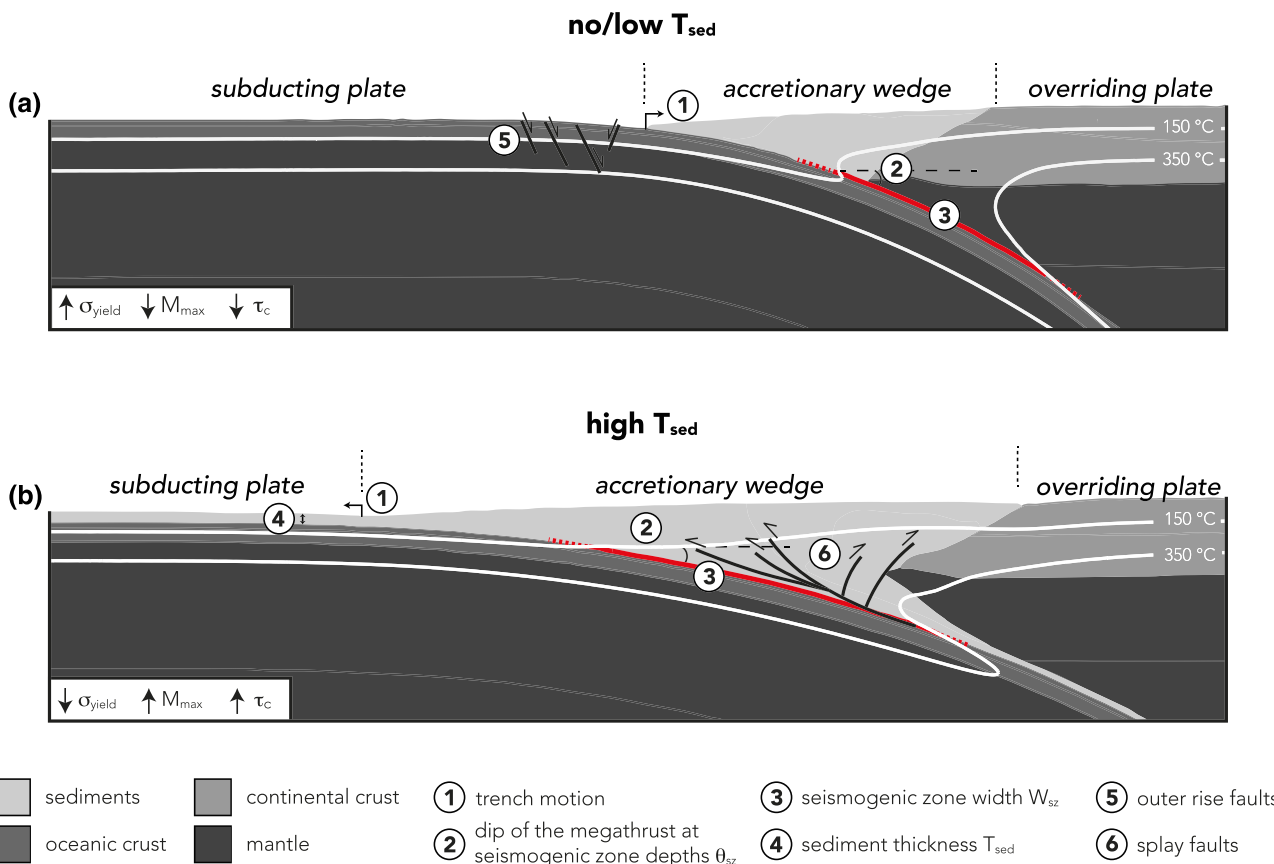


Figure 9. Effect of sediment thickness T_{sed} on long- and short-term behavior of subduction zones. (a) no/low, and (b) high T_{sed} . The white lines mark the 150°C and 350°C isotherms, where the subduction megathrust has seismogenic (i.e., velocity-weakening) behavior. σ_{yield} is the yield strength of the megathrust, M_{max} is the maximum moment magnitude of megathrust earthquakes, and τ_c is the recurrence time of the characteristic events. The upward- and downward-pointing arrows depict an increase and a decrease for increasing T_{sed} , respectively.

4.2. How Does Sediment Thickness Affect Long-Term Subduction Behavior?

4.2.1. Megathrust Seismogenic Zone Geometry

Our results show that the megathrust dip is shallower for large incoming plate sediment thickness (Figures 3 and 4b). As more and more sediments accumulate near the trench during subduction, the volume of material that needs to be accommodated in front of the preexisting sedimentary wedge increases. This is most easily accommodated via the seaward growth of the wedge, which becomes larger with more incoming plate sediments (Figure 3). Thus, we observe significant trench retreat (Figure 3). However, the slab at depth remains at approximately the same location (Movie S1). This observation suggests that trench retreat in our model is enhanced by the development of a larger sedimentary wedge. As slab retreat is negligible during the seaward motion of the trench caused by the frontal accretion of sediments, the curvature radius of the slab increases and the seismogenic portion of the megathrust flattens during subduction. Additionally, the added weight exerted by large amounts of sediments on the seaward side of the margin promotes slab unbending through time (Movie S1). As a result, we observe a decrease of the megathrust dip (Figure 4b) and, in turn, an increase of the seismogenic zone width (Figure 4c). This increase mainly results from the decrease in the slab dip and not from a change in the seismogenic zone depth range, since isotherm shallowing mostly occurs through an equal upward translation of both the updip and downdip limit (Figure 4a).

The decrease in the interface strength caused by increasing sediments (Figure 4d) may have also favored a shallower megathrust dip and consequently a wider seismogenic zone through a feedback on trench retreat. This is because a decrease of the interface strength likely decreases the mechanical coupling between the subducting and overriding plates, hence contributing to slab and trench retreat. However, since slab

retreat is negligible in our models (Movie S1), we infer that interface strength has affected trench kinematics to a lesser extent.

To test whether the feedback between incoming plate sediment thickness and long-term subduction behavior also holds in nature, we compare our numerical results to the global subduction zone characteristics database that includes physical and seismological observations of 62 subduction segments (Heuret et al., 2012, 2011). The correlation between trench motion and amount of sediments is not significant for natural data (Figure S2b). However, the amount of trench motion in our models could be influenced by a combination of adopted variables (e.g., slab density, viscosity, and thickness; Bellahsen, 2005; Schellart et al., 2007) and boundary conditions (e.g., Funiciello et al., 2004; Heuret et al., 2007).

The relationship between sediment thickness, dip, and width of the megathrust has a similar trend in our models and nature (Figures 4b and 4c). Pearson's correlation coefficients are lower than in our models and indicate a moderate correlation (i.e., $R = 0.59$ and 0.53 for θ_{sz} and W_{sz} , respectively). Therefore, the amount of subducting sediments influences subduction zone geometry, as shallow dipping (i.e., θ_{sz} between 9° and 15°) megathrusts with wide seismogenic zones (i.e., W_{sz} between 130 and 250 km) are most often associated with sediment-rich (i.e., $T_{sed} \geq 1$ km) subduction segments. The wider data scattering for natural subduction zones is expected, as the observed variability in our models depends only on the amount of sediments, while slab geometry in nature is affected by many other factors (e.g., Lallemand et al., 2005) that are not included in this study.

4.2.2. Megathrust Strength

Our results show that the megathrust is on average weaker when more sediments are subducting (Figure 4d). This decrease in the average yield strength of the interface (i.e., the sediment-basalt transition, where megathrust ruptures propagate) for increasing amounts of sediments may occur due to several reasons.

One commonly assumed reason is that sediments have a lower (static) friction coefficient compared to the surrounding rocks. The frictional strength of the megathrust along the sediment-basalt interface would thus be readily decreased. However, the difference in static friction becomes less relevant, as a small amount of sediments is always present along the interface including for an initial sediment thickness of 0 km (Figure 3a) due to the basal erosion of the sedimentary wedge.

A more relevant contribution to the progressive weakening of the interface for thicker sediments is related to a decrease of lithostatic pressure that occurs due to the shallowing of the isotherms (Figure 4a). This interpretation is supported by the observation of predominant lithostatic pressure of the basalt-sediments interface at seismogenic zone depths. The relevant change in isotherm depth at this location is actually caused by the difference in the initial temperature field of the oceanic plate as it enters at the trench. As the incoming plate sediment thickness increases, the initial temperature at the top of the basalt increases as well (i.e., $T \sim 0^\circ\text{C}$ for $T_{sed} = 0$ km and $T \sim 150^\circ\text{C}$ for $T_{sed} = 8$ km; Figure 3). Therefore, the interface of future ruptures in a setting with thick sediments is already much warmer as soon as the oceanic plate enters at the trench. The initially warmer interface thus causes a shallower location of both the updip and downdip limits (i.e., the 150°C and 350°C isotherms, respectively) of the seismogenic zone. Due to the shallower isotherms, the average lithostatic pressure in the seismogenic zone is lower. This results in a decrease of the interface yield strength, which therefore produces a weaker megathrust. Assuming lithostatic pressures, we estimate that seismogenic zone shallowing related to the increase of incoming plate sediments can decrease the megathrust yield strength by $\sim 24\%$.

One could argue that a warmer interface could also result from the larger amount of radiogenic heat that more incoming plate sediments produce (Table 1). However, we find that the effect of radiogenic heat on isotherms shallowing as observed on the basalt-sediment transition in our models is negligible (i.e., upward shift of only 4 km of the 350°C isotherm; Figure S4).

An additional feedback mechanism that influences the interface strength occurs through a change in the average density of the overlying forearc. When sediments are not present, most of the seismogenic zone lies below the dense lithospheric mantle of the overriding plate (Figure 3a). Increasing the sediment thickness on the incoming plate results in the development of a wide sedimentary prism, entirely overlying the seismogenic interface (Figure 3d). Due to such a lighter forearc structure, the vertical component of the pressure and the normal stress acting on the interface decreases, and so does the yield strength (Figure 4d).

Assuming a density of 2,600 and 3,000 kg m⁻³ for sediments and basaltic crust (Table 1), we estimate that density variations of the forearc can decrease the megathrust yield strength by ~13%.

4.3. How Does Sediment Thickness Affect Megathrust Seismicity?

Our results support the hypothesis that the amount of sediments on the incoming plate plays an important role on megathrust seismicity (e.g., Brizzi et al., 2018; Heuret et al., 2012; Scholl et al., 2015; Seno, 2017; Ruff, 1989). This is because of the long-term effect that sediment subduction has on the geometry of the megathrust. We show that the seismogenic zone gets wider with increasing incoming plate sediment thickness (Figures 3 and 4c). As a result, the potential rupture area increases as well. Several authors have already suggested that sediments may promote rupture propagation over long trench-parallel distances by providing homogeneous strength conditions due to the smoothening of the seafloor roughness (Brizzi et al., 2018; Heuret et al., 2012; Ruff, 1989; Scholl et al., 2015). Additionally, sediments may lubricate the megathrust, thus enhancing slip propagation (e.g., Sawai et al., 2014). Here, we point out that sediments may also enhance ruptures to grow larger in the downdip direction, given the wider seismogenic zone that develops due to the feedback between sediment thickness and megathrust geometry. This new additional effect operates in the same direction as the smoothening and lubricating effects proposed by previous studies. Sediment-rich subduction zones may thus be more prone to host giant earthquakes, given that the potential rupture area is larger. Additionally, the negligible slab retreat in our models would tentatively suggest that the upper plate is characterized by a neutral strain regime. This would support the outcomes of Heuret et al. (2012) that giant earthquakes preferentially occur at subduction zones that combine large sediment thickness and neutral upper plate strain.

On a global-scale, giant earthquakes seem to preferentially occur at subduction zones with high sediment supply (Figure 1; Brizzi et al., 2018; Heuret et al., 2012; Ruff, 1989; Scholl et al., 2015). However, there are exceptions to this trend, as giant events have also occurred at relatively sediment-starved margins (Figure 1). A clear example of such an exception is the Japanese subduction segment. This hosted the 2011 Tōhoku-Oki earthquake, which reached a M_w of 9.0 although the amount of trench sediments is relatively low (i.e., $T_{\text{sed}} = 0.8 \text{ km}$ Heuret et al., 2012). This event has shown unusual characteristics compared to, for example, the 1960 Chile and 2004 Sumatra earthquakes, namely, the large amount of slip in a relatively small rupture area and shallow rupture propagation (e.g., Stimpson, 2011). This points out that other processes, such as thermal pressurization (e.g., Noda & Lapusta, 2013) and dynamic overshoot (e.g., Ide et al., 2011), certainly play a role in the generation of large megathrust earthquakes.

Sediment-rich subduction segments that have not generated a giant earthquake within our instrumental observation time window of ~110 years are also exceptions (Figure 1). In fact, the maximum magnitude of Makran, West-Aegean, and Calabria segments, which have the thickest trench fill ($T_{\text{sed}} \geq 5 \text{ km}$ Heuret et al., 2012), is relatively low (i.e., 8.1, 7.7, and 7.2, respectively). However, the occurrence of giant earthquakes at Makran, West-Aegean and Calabria segments may not be unlikely. Our results show that giant events occur in subduction margins with thick incoming plate sediments, and that the recurrence time of these large characteristic events is significantly increased (Figure 7b). Furthermore, the corresponding wide seismogenic zone causes the megathrust to have irregular recurrence behavior (Figures 6d and 7b), similar to what has been previously described as supercycles (e.g., Herrendörfer et al., 2015). For these large seismogenic widths, we thus observe the occurrence of partial ruptures with relatively low magnitude, which alternate with the complete failure of the entire seismogenic zone (e.g., Herrendörfer et al., 2015). This transition from quasi-periodic characteristic ruptures to the additional occurrence of partial ruptures is also predicted by recent analytical and numerical models (Barbot, 2019; Cattania, 2019) for regions with large seismogenic zone widths over critical nucleation sizes. This irregular behavior for thicker sediments could help to explain the weak relationship between the maximum magnitude of megathrust earthquakes and sediment thickness in natural subduction zones ($R < 0.1$; Figure 7a), as historical and instrumental data are only available for a limited time window (McCaffrey, 2008). More importantly, our findings suggests that the Makran, West-Aegean, and Calabria segments may be at the stage when only smaller partial ruptures occur and their recorded M_{max} may not be representative of the largest possible megathrust earthquake. If this scenario is correct, we speculate that they may host giant earthquakes in the future.

4.4. How Does Sediment Thickness Affect Off-Megathrust Seismicity?

The amount of incoming plate sediments also affects subduction intraplate seismicity (Figure 5). In the case of low sediments (i.e., $T_{\text{sed}} < 1.5$ km), we observe a higher number of outer rise events (Figures 5a-5b, and S3). This is because thin sediments are associated with a steeper megathrust dip and thus increased bending of the slab. More bending increases the extensional stresses in the shallow part of the slab and thus increases the amount of normal faulting earthquakes within the outer rise. In contrast, models with thick sediments (i.e., $T_{\text{sed}} > 4$ km; Figures 5d and S3) show a higher number of splay faults branching off from the megathrust, likely because of the development of a larger sedimentary wedge. Therefore, our results suggest that the amount of sediments also influences where seismic energy is preferentially released outside of the megathrust. For example, our models predict that the seismic moment released by faulting in the sedimentary wedge is higher in sediment-rich subduction segments than in sediment-poor ones. They also predict that the ratio of seismic moment release in the upper plate and in the lower plate is higher for subduction segments with more incoming sediments. However, further investigation is needed to support this hypothesis. A future expansion of the global subduction zone database (Heuret et al., 2011, 2012) that includes intraplate seismicity (Presti et al., 2012) could be used to test our predicted relationships between the amount of sediments and off-megathrust faulting.

4.5. Impact of Subduction Dynamics on Megathrust Seismicity

In numerical simulations, the presence and effect of sediments along the megathrust is typically approximated by assuming a low friction coefficient at the interface (e.g., Muldashev, 2017; Tan et al., 2012). Hence, sediments are usually not included as a physical layer, but parameterized as a frictionally weak material. Given the strong feedback between long-term sediment subduction and megathrust seismicity highlighted by our models, we tested to what extent the presence of sediments influences the tectonic evolution of subduction zones and, in turn, the short-term behavior of megathrust. To do so, we ran an additional model in which we lower the static friction coefficient μ_s of the plate interface to parameterize the presence of sediments instead of explicitly modeling them as a layer. We show that μ_s of the plate interface controls subduction geometry, with shallower dipping slabs and wider seismogenic zones for lower friction (Figures 4b and 4c). This is in agreement with previous geodynamic modeling studies, which show that the subduction megathrust has a shallow dip and a wide seismogenic zone in the case of low sediment friction (Tan et al., 2012).

Tuning the interface frictional properties, however, results in a lower variability of the megathrust geometry compared to what is observed when increasing the sediment thickness. This outcome has significant implications for the maximum size of earthquakes M_{max} that the megathrust can generate (Figure 8). We show that M_{max} of megathrust events increases by ~ 1 order of magnitude as a function of sediment thickness. If sediments are instead simulated by assuming a frictionally weak interface, M_{max} varies over a much smaller range of 0.1 magnitude. Therefore, the absence of a physical layer of sediments results in a notable underestimation of the maximum earthquake size the megathrust can generate.

We expect that the M_{max} variation is even smaller in a simplified mechanical approach that only varies friction and does not include long-term subduction dynamics and thermal coupling, such as in spring-slider experiments (e.g., Corbi et al., 2011). In this case, the seismogenic zone width does not vary as a function of friction coefficient or sediment presence. This means that the maximum magnitude of megathrust earthquakes over multiple seismic cycles does not vary either, as the maximum potential slip area is fixed (Figure 8). However, in our interpretation we still allow for a minor variation of M_{max} (Figure 8), since the rupture width could vary slightly if analyzed using a similar slip rate threshold as done for the other two scenarios.

Our results demonstrate for the first time the distinct impact and importance of long-term subduction dynamics on the short-term behavior of megathrusts. A difference of ~ 1 order of magnitude when estimating M_{max} is in fact significant for correctly assessing earthquake hazard. This was clearly demonstrated by the 2011 Tōhoku-Oki earthquake and associated tsunami. Historically, many M_w 7–8 earthquakes have occurred on the Japanese megathrust, but a giant event that was 1 order of magnitude higher was not expected in this region (e.g., Stein & Okal, 2011), and neither was the associated tsunami. The waves generated by the seafloor displacement were higher than expected and overtopped the antitsunami walls of the

Fukushima Daiichi nuclear power plant, penetrating far inland and causing enormous damage (e.g., Stimpson, 2011). Including a sedimentary layer in numerical models is thus important for improving estimates of the magnitude of future earthquakes to mitigate the seismic hazard of subduction zones.

5. Conclusions

We have isolated and quantified the contribution of incoming plate sediment thickness on the long- and short-term behavior of subduction zones using STM models.

We find that the trench significantly retreats due to the seaward growth of the sedimentary wedge when more sediments subduct. This retreating trench motion in combination with a negligible slab retreat at depth causes the megathrust to flatten. Concurrently, the additional weight of sediments favors slab unbending. Therefore, thick incoming plate sediments enhance the development of a shallower dipping megathrust, which has a wider seismogenic zone. Comparison with natural data supports that sediment-rich subduction segments are often characterized by a shallower interface dip and larger seismogenic zone width than the sediment-starved ones.

We also find that the megathrust is on average weaker for increasing sediment thickness. This is mainly due to a shallower seismogenic zone and a lighter forearc structure that decrease the pressure and the normal stress acting on the interface.

We show that the maximum magnitude of megathrust earthquakes increases with increasing sediments. This supports the hypothesis that the amount of sediments influences giant earthquakes occurrence. Based on our findings, we propose an additional explanation for the impact of sediment thickness on the maximum size of megathrust earthquakes. Besides smoothing and lubricating the plate interface, we suggest that thick sediments increase the potential slip area by increasing the seismogenic zone width. This may also promote earthquakes to grow larger and reach higher magnitudes. For the subduction segments with the thickest trench infill (Makran, Calabria, and West-Aegean), the maximum magnitude of megathrust earthquakes predicted by our models is significantly higher than what has been observed during the last century. Considering the increased recurrence time of the characteristic events for high amounts of sediments, in combination with a more irregular recurrence behavior that causes the megathrust to also generate partial ruptures, we suggest that larger than expected earthquakes may still occur in these regions, albeit infrequently.

We further find that increasing the sediment thickness causes the intraplate seismicity to migrate from the outer rise region to the sedimentary wedge. Thin incoming plate sediments result in a steeper megathrust, more slab bending, thereby more outer rise earthquakes. As the sediment thickness increases, slab bending decreases, the sedimentary wedge gets wider, and this results in more events propagating along splay faults. The amount of sediments thus dictates how seismic energy is partitioned off-megathrust.

Finally, we have quantified the importance of simulating long-term sediment subduction in contrast to the parameterization of sediments through a frictionally weak megathrust. We show that a significant underestimation of the maximum earthquake size of up to one order of magnitude could occur if long-term subduction dynamics, the physical presence of sediments and thermal coupling are ignored. This strengthens how crucial it is to bridge the time scales from tectonic evolution to earthquakes to improve seismic hazard assessment at subduction zones.

Data Availability Statement

Numerical simulations were run on CSCS cluster Mönch under project s741. The model executables, input files, and outputs for the model with $T_{\text{sed}} = 4 \text{ km}$ are available through Zenodo data repository under the Creative Commons Licence: Attribution 4.0 International and published open access in Brizzi et al. (2020). Figures 5 and 6 were made using the perceptually uniform colormap Imola by Cramer (2018).

References

- Allmann, B. P., & Shearer, P. M. (2009). Global variations of stress drop for moderate to large earthquakes. *Journal of Geophysical Research*, 114, B01310. <https://doi.org/10.1029/2008JB005821>

Acknowledgments

We thank the Editor Uri ten Brink, the Associate Editor and reviewer Sasha Brune and an anonymous reviewer for providing detailed and constructive comments. We are grateful to Elenora van Rijssingen, Claudio Petrini, Casper Pranger, Marie Bocher and Luca Dal Zilio for fruitful discussions that improved the quality of the manuscript. Luca Dal Zilio is also thanked for providing the RDA algorithm. The grant provided to the Department of Science, Roma Tre University (MIUR-ITALY Dipartimenti di Eccellenza, ARTICOLO 1, COMMI 314-337 LEGGE 232/2016) is also gratefully acknowledged.

- Ampuero, J.-P., & Ben-Zion, Y. (2008). Cracks, pulses and macroscopic asymmetry of dynamic rupture on a bimaterial interface with velocity-weakening friction. *Geophysical Journal International*, 173(2), 674–692. <https://doi.org/10.1111/j.1365-246X.2008.03736.x>
- Audet, P., & Schwartz, S. Y. (2013). Hydrologic control of forearc strength and seismicity in the Costa Rican subduction zone. *Nature Geoscience*, 6(10), 852–855. <https://doi.org/10.1038/ngeo1927>
- Barbot, S. (2019). Slow-slip, slow earthquakes, period-two cycles, full and partial ruptures, and deterministic chaos in a single asperity fault. *Tectonophysics*, 768, 228171.
- Bellahsen, N. (2005). Dynamics of subduction and plate motion in laboratory experiments: Insights into the “plate tectonics” behavior of the Earth. *Journal of Geophysical Research*, 110, B01401. <https://doi.org/10.1029/2004JB002999>
- Blaser, L., Krüger, F., Ohrnberger, M., & Scherbaum, F. (2010). Scaling relations of earthquake source parameter estimates with special focus on subduction environment. *Bulletin of the Seismological Society of America*, 100(6), 2914–2926.
- Brizzi, S., Sandri, L., Funiciello, F., Corbi, F., Piromallo, C., & Heuret, A. (2018). Multivariate statistical analysis to investigate the subduction zone parameters favoring the occurrence of giant megathrust earthquakes. *Tectonophysics*, 728–729.
- Brizzi, S., van Zelst, I., Funiciello, F., Corbi, F., & van Dinther, Y. (2020). Model data repository of “How sediment thickness influences subduction dynamics and seismicity” [Data set]. Zenodo. <http://doi.org/10.5281/zenodo.3866654>
- Cattania, C. (2019). Complex earthquake sequences on simple faults. *Geophysical Research Letters*, 46, 10,384–10,393. <https://doi.org/10.1029/2019GL083628>
- Chester, F. M., & Higgs, N. G. (1992). Multimechanism friction constitutive model for ultrafine quartz gouge at hypocentral conditions. *Journal of Geophysical Research*, 97(B2), 1859–1870. <https://doi.org/10.1029/91JB02349>
- Chester, M., James J., Toczko, S., Eguchi, N., Kido, Y., Saito, S., et al. (2012). Integrated Ocean Drilling Program Expedition 343/343T Preliminary Report, Japan Trench Fast Drilling Project (JFAST), 1 April 24 May 2012 and 5–19 July 2012 (Vol. 343; Tech. Rep.)
- Corbi, F., Funiciello, F., Faccenna, C., Ranalli, G., & Heuret, A. (2011). Seismic variability of subduction thrust faults: Insights from laboratory models. *Journal of Geophysical Research*, 116, B06304. <https://doi.org/10.1029/2010JB007993>
- Cramer, F. (2018). Scientific colour-maps: Zenodo. <https://doi.org/10.5281/zenodo.1243862>
- Cramer, F., Schmeling, H., Golabek, G. J., Duretz, T., Orendt, R., Buitier, S. J. H., et al. (2012). A comparison of numerical surface topography calculations in geodynamic modelling: An evaluation of the ‘sticky air’ method. *Geophysical Journal International*, 189(1), 38–54.
- Dal Zilio, L., van Dinther, Y., Gerya, T. V., & Pranger, C. C. (2018). Seismic behaviour of mountain belts controlled by plate convergence rate. *Earth and Planetary Science Letters*, 482, 81–92. <https://doi.org/10.1016/j.epsl.2017.10.053>
- Del Gaudio, P., Di Toro, G., Han, R., Hirose, T., Nielsen, S., Shimamoto, T., & Cavallo, A. (2009). Frictional melting of peridotite and seismic slip. *Journal of Geophysical Research*, 114, B06306. <https://doi.org/10.1029/2008JB005990>
- Den Hartog, S. A. M., Niemeijer, A. R., & Spiers, C. J. (2012). New constraints on megathrust slip stability under subduction zone P-T conditions. *Earth and Planetary Science Letters*, 353, 240–252. <https://doi.org/10.1016/j.epsl.2012.08.022>
- Di Toro, G., Han, R., Hirose, T., De Paola, N., Nielsen, S., Mizoguchi, K., et al. (2011). Fault lubrication during earthquakes. *Nature*, 471(7339), 494. <https://doi.org/10.1038/nature09838>
- Fagereng, Å. (2011). Wedge geometry, mechanical strength, and interseismic coupling of the Hikurangi subduction thrust, New Zealand. *Tectonophysics*, 507(1–4), 26–30. <https://doi.org/10.1016/j.tecto.2011.05.004>
- Funiciello, F., Faccenna, C., & Giardini, D. (2004). Role of lateral mantle flow in the evolution of subduction systems: Insights from laboratory experiments. *Geophysical Journal International*, 157(3), 1393–1406. <https://doi.org/10.1111/j.1365-246X.2004.02313.x>
- Gao, X., & Wang, K. (2017). Rheological separation of the megathrust seismogenic zone and episodic tremor and slip. *Nature*, 543(7645), 416–419. <https://doi.org/10.1038/nature21389>
- Gerya, T. V. (2019). *Introduction to numerical geodynamic modelling*: Cambridge University Press.
- Gerya, T. V., & Meilick, F. I. (2011). Geodynamic regimes of subduction under an active margin: Effects of rheological weakening by fluids and melts. *Journal of Metamorphic Geology*, 29(1), 7–31. <https://doi.org/10.1111/j.1525-1314.2010.00904.x>
- Gerya, T. V., & Yuen, D. A. (2007). Robust characteristics method for modelling multiphase visco-elasto-plastic thermo-mechanical problems. *Physics of the Earth and Planetary Interiors*, 163(1–4), 83–105.
- Gorczyk, W., Willner, A. P., Gerya, T. V., Connolly, J. A. D., & Burg, J. P. (2007). Physical controls of magmatic productivity at Pacific-type convergent margins: Numerical modelling. *Physics of the Earth and Planetary Interiors*, 163(1–4), 209–232.
- Gulick, S. P. S., Austin, J. A., McNeill, L. C., Bangs, N. L. B., Martin, K. M., Henstock, T. J., et al. (2011). Updip rupture of the 2004 Sumatra earthquake extended by thick indurated sediments. *Nature Geoscience*, 4(7), 453–456. <https://doi.org/10.1038/NGEO1176>
- Han, S., Bangs, N. L., Carbotte, S. M., Saffer, D. M., & Gibson, J. C. (2017). Links between sediment consolidation and Cascadia megathrust slip behaviour. *Nature Geoscience*, 10(12), 954–959. <https://doi.org/10.1038/s41561-017-0007-2>
- Herrendörfer, R., van Dinther, Y., Gerya, T. V., & Dalguer, L. A. (2015). Earthquake supercycle in subduction zones controlled by the width of the seismogenic zone. *Nature Geoscience*, 8(6), 471–474. <https://doi.org/10.1038/ngeo2427>
- Heuret, A., Conrad, C. P., Funiciello, F., Lallemand, S., & Sandri, L. (2012). Relation between subduction megathrust earthquakes, trench sediment thickness and upper plate strain. *Geophysical Research Letters*, 39, L05304. <https://doi.org/10.1029/2011GL050712>
- Heuret, A., Funiciello, F., Faccenna, C., & Lallemand, S. (2007). Plate kinematics, slab shape and back-arc stress: A comparison between laboratory models and current subduction zones. *Earth and Planetary Science Letters*, 256(3–4), 473–483. <https://doi.org/10.1016/j.epsl.2007.02.004>
- Heuret, A., Lallemand, S., Funiciello, F., Piromallo, C., & Faccenna, C. (2011). Physical characteristics of subduction interface type seismogenic zones revisited. *Geochemistry, Geophysics, Geosystems*, 12, Q01004. <https://doi.org/10.1029/2010GC003230>
- Hyndman, Yamano, M., & Oleskevich, D. A. (1997). The seismogenic zone of subduction thrust faults. *Island Arc*, 6(3), 244–260. <https://doi.org/10.1111/j.1440-1738.1997.tb00175.xpredicted>
- Ide, S., Baltay, A., & Beroza, G. C. (2011). Shallow dynamic overshoot and energetic deep rupture in the 2011 Mw 9.0 Tohoku-Oki earthquake. *Science*, 332(6036), 1426–1429. <https://doi.org/10.1126/science.1207020>
- Lallemand, S., Heuret, A., & Boutelier, D. (2005). On the relationships between slab dip, back-arc stress, upper plate absolute motion, and crustal nature in subduction zones. *Geochemistry, Geophysics, Geosystems*, 6, Q09006. <https://doi.org/10.1029/2005GC000917>
- Lallemand, S., Peyret, M., van Rijsingen, E., Arcay, D., & Heuret, A. (2018). Roughness characteristics of oceanic seafloor prior to subduction in relation to the seismogenic potential of subduction zones. *Geochemistry, Geophysics, Geosystems*, 19, 2121–2146. <https://doi.org/10.1029/2018GC007434>
- Lamb, S., & Davis, P. (2003). Cenozoic climate change as a possible cause for the rise of the Andes. *Nature*, 425(6960), 792–797. <https://doi.org/10.1038/nature02049>
- McCaffrey, R. (2008). Global frequency of magnitude 9 earthquakes. *Geology*, 36(3), 263–266.

- Moreno, M., Haberland, C., Oncken, O., Rietbrock, A., Angiboust, S., & Heidbach, O. (2014). Locking of the Chile subduction zone controlled by fluid pressure before the 2010 earthquake. *Nature Geoscience*, 7(4), 292–296. <https://doi.org/10.1038/ngeo2102>
- Moreno, M., Li, S., Melnick, D., Bedford, J. R., Baez, J. C., Motagh, M., et al. (2018). Chilean megathrust earthquake recurrence linked to frictional contrast at depth. *Nature Geoscience*, 11(4), 285–290. <https://doi.org/10.1038/s41561-018-0089-5>
- Muldashov, I. (2017). Modeling of the great earthquake seismic cycles (PhD Thesis), Potsdam.
- Noda, H., & Lapusta, N. (2013). Stable creeping fault segments can become destructive as a result of dynamic weakening. *Nature*, 493(7433), 518–521. <https://doi.org/10.1038/nature11703>
- Olsen, K. M., Bangs, N. L., Tréhu, A. M., Han, S., Arnulf, A., & Contreras-Reyes, E. (2020). Thick, strong sediment subduction along south-central Chile and its role in great earthquakes. *Earth and Planetary Science Letters*, 538, 116,195. <https://doi.org/10.1016/j.epsl.2020.116195>
- Presti, D., Heuret, A., Funiciello, F., & Piromallo, C. (2012). A new database on subduction seismicity at the global scale, *Egu general assembly conference abstracts* (Vol. 14, pp. 2277).
- Ranalli, G. (1995). *Rheology of the Earth* (2nd Ed.). Chapman and Hall.
- Ruff, L. J. (1989). Do trench sediments affect great earthquake occurrence in subduction zones? *Pure and Applied Geophysics*, 129(1-2), 263–282.
- Saffer, D. M., & Marone, C. (2003). Comparison of smectite- and illite-rich gouge frictional properties: Application to the updip limit of the seismogenic zone along subduction megathrusts. *Earth and Planetary Science Letters*, 215, 219–235. [https://doi.org/10.1016/S0012-821X\(03\)00424-2](https://doi.org/10.1016/S0012-821X(03)00424-2)
- Saffer, D. M., & Tobin, H. J. (2011). Hydrogeology and mechanics of subduction zone forearcs: Fluid flow and pore pressure. *Annual Review of Earth and Planetary Sciences*, 39, 157–186. <https://doi.org/10.1146/annurev-earth-040610-133408>
- Sawai, M., Hirose, T., & Kameda, J. (2014). Frictional properties of incoming pelagic sediments at the Japan Trench: Implications for large slip at a shallow plate boundary during the 2011 Tohoku earthquake. *Earth, Planets and Space*, 66, 65. <https://doi.org/10.1186/1880-5981-66-65>
- Schellart, W. P., Freeman, J., Stegman, D. R., Moresi, L., & May, D. (2007). Evolution and diversity of subduction zones controlled by slab width. *Nature*, 446(7133), 308–311. <https://doi.org/10.1038/nature05615>
- Scholl, D. W., Kirby, S. H., von Huene, R., Ryan, H., Wells, R. E., & Geist, E. L. (2015). Great ($\geq M_w 8.0$) megathrust earthquakes and the subduction of excess sediment and bathymetrically smooth seafloor. *Geosphere*, 11(2), 236–265.
- Schlitz, R. (1995). Limits on strength and deformation properties of jointed basaltic rock masses. *Rock Mechanics and Rock Engineering*, 28(1), 1–15. <https://doi.org/10.1007/BF01024770>
- Seno, T. (2009). Determination of the pore fluid pressure ratio at seismogenic megathrusts in subduction zones: Implications for strength of asperities and Andean-type mountain building. *Journal of Geophysical Research*, 114, B05405. <https://doi.org/10.1029/2008JB005889>
- Seno, T. (2017). Subducted sediment thickness and $M_w 9$ earthquakes. *Journal of Geophysical Research: Solid Earth*, 122, 470–491. <https://doi.org/10.1002/2016JB013048>
- Stein, S., & Okal, E. A. (2011). The size of the 2011 Tohoku earthquake need not have been a surprise. *Eos, Transactions, American Geophysical Union*, 92(27), 227–228. <https://doi.org/10.1029/2011EO270005>
- Stimpson, I. (2011). Japan's tohoku earthquake and tsunami. *Geology Today*, 27(3), 96–98. <https://doi.org/10.1111/j.1365-2451.2011.00793.x>
- Tan, E., Lavier, L. L., Van Avendonk, H. J. A., & Heuret, A. (2012). The role of frictional strength on plate coupling at the subduction interface. *Geochemistry, Geophysics, Geosystems*, 13, Q10006. <https://doi.org/10.1029/2012GC004214>
- Tsutsumi, A., & Shimamoto, T. (1997). High-velocity frictional properties of gabbro. *Geophysical Research Letters*, 24(6), 699–702. <https://doi.org/10.1029/97GL00503>
- Turcotte, D. L., & Schubert, G. (2002). *Geodynamics*. New York: Cambridge University Press.
- van Dinther, Y., Gerya, T. V., Dalguer, L. A., Corbi, F., Funiciello, F., & Mai, P. M. (2013). The seismic cycle at subduction thrusts: 2. Dynamic implications of geodynamic simulations validated with laboratory models. *Journal of Geophysical Research: Solid Earth*, 118, 1502–1525. <https://doi.org/10.1029/2012JB009479>
- van Dinther, Y., Gerya, T. V., Dalguer, L. A., Mai, P. M., Morra, G., & Giardini, D. (2013). The seismic cycle at subduction thrusts: Insights from seismo-thermo-mechanical models. *Journal of Geophysical Research: Solid Earth*, 118, 6183–6202. <https://doi.org/10.1002/2013JB010380>
- van Dinther, Y., Mai, P. M., Dalguer, L. A., & Gerya, T. V. (2014). Modeling the seismic cycle in subduction zones: The role and spatio-temporal occurrence of off-megathrust earthquakes. *Geophysical Research Letters*, 41, 1194–1201. <https://doi.org/10.1002/2013GL058886>
- van Rijsingen, E., Lallemand, S., Peyret, M., Arcay, D., Heuret, A., Funiciello, F., & Corbi, F. (2018). How subduction interface roughness influences the occurrence of large interplate earthquakes. *Geochemistry, Geophysics, Geosystems*, 19, 2342–2370. <https://doi.org/10.1029/2018GC007618>
- van Zelst, I., Wollherr, S., Gabriel, A.-A., Madden, E. H., & van Dinther, Y. (2019). Modeling megathrust earthquakes across scales: One-way coupling from geodynamics and seismic cycles to dynamic rupture. *Journal of Geophysical Research: Solid Earth*, 124, 11,414–11,446. <https://doi.org/10.1029/2019JB017539>
- Wang, K., & Bilek, S. L. (2014). Invited review paper: Fault creep caused by subduction of rough seafloor relief. *Tectonophysics*, 610, 1–24.